Composites Part B 186 (2020) 107827

Contents lists available at ScienceDirect

Composites Part B

journal homepage: www.elsevier.com/locate/compositesb

Fluorine/adamantane modified cyanate resins with wonderful interfacial bonding strength with PBO fibers

Lin Tang [a,1], Junliang Zhang [a,c,1], Yusheng Tang [a,**], Yuxiao Zhou [a], Yuhan Lin [a], Zheng Liu [a], Jie Kong [a], Tianxi Liu [b], Junwei Gu [a,*]

[a] Shaanxi Key Laboratory of Macromolecular Science and Technology, School of Chemistry and Chemical Engineering, Northwestern Polytechnical University, Xi' an, Shaanxi, 710072, PR China
[b] State Key Laboratory for Modification of Chemical Fibers and Polymer Materials, Donghua University, Shanghai, 201620, PR China
[c] School of Materials Science and Engineering, Henan University of Science and Technology, Luoyang, 471023, PR China

ARTICLE INFO

Keywords:
Fluorine/adamantane
Bisphenol A cyanate ester (BADCy)
Dielectric properties
Heat resistance
Interfacial compatibility

ABSTRACT

Novel compound (AEAF) with both cage-type adamantanes and fluorine-containing structures was synthesized from bisphenol AF, 1-adamantyl chloride and epichlorohydrin through successive esterification and O-alkylation reaction, which was then introduced into the curing networks of bisphenol A cyanate ester (BADCy) resins through copolymerization, to obtain AEAF-*co*-BADCy resins. AEAF presented low polarizability & dipole density, rigid cage adamantane, and stable CF_3 group. When the mass fraction of AEAF was 6 wt%, AEAF-*co*-BADCy resins displayed the minimum real part (ε'_r), imaginary part (ε''_r) of complex permittivity, and dielectric loss tangent ($tan\delta$) values, which were 2.49, 0.012, and 0.0048, respectively. And the corresponding wave transmission efficiency (T) was 92.3%, significantly higher than that of pure BADCy (86.6%). AEAF-*co*-BADCy resins also possessed excellent mechanical properties and better interfacial compatibilities with poly(*p*-phenylene-2,6-benzobisoxazole) (PBO) fibers. The corresponding flexural strength (126.5 MPa) and impact strength (15.2 kJ m^{-2}) were increased by 16.6% and 47.6%, in comparison to pure BADCy (flexural strength of 108.5 MPa and impact strength of 10.3 kJ m^{-2}). Meantime, the single fiber pull-out strength of PBO fibers/AEAF-*co*-BADCy (6 wt% AEAF) micro-composites also displayed an increase from 3.1 MPa (PBO fibers/BADCy) to 3.4 MPa.

1. Introduction

High-performance cyanate ester (CE) resins are widely used in the fields of radome, printed circuit board (PCB), and electronic communications, *etc* [1–4]. Dielectric properties of CE resins are important parameters for evaluating the wave transmission efficiency. In comparison to unsaturated polyester (UP) [5], bismaleimide (BMI) [6], polyimide (PI) [7], and epoxy resin (EP) [8], CE resins possess better wave transmission efficiency due to low dielectric constant (ε, 2.6–3.2) and dielectric loss tangent ($tan\delta$, 0.005–0.010) over wide temperatures and frequencies ranges [9–11]. What's more, CE resins not only possess excellent heat & chemical resistance, but also high glass transition temperature (T_g), low coefficient of expansion, and good processability [12–15]. However, with the rapid development of electronic information technology, high quality CE resins [16] and their composites [17] with lightweight, ultra-high wave transmission efficiency (ultra-low ε and $tan\delta$ values), superior heat & moist heat resistance, and outstanding mechanical properties are crucially needed in order to meet the increasing requirements for novel wave-transparent polymer composites.

To date, common method for increasing wave transmission efficiency of polymers and polymer composites is reducing the values of ε and $tan\delta$ values [18]. Common approach to decrease ε and $tan\delta$ values of CE resins is by reducing the density and molecular polarizability of polarized molecules [19–21]. For example, introducing nano-sized pores into the CE resins, through physical or chemical methods, can effectively reduce the density of polarized molecules. Both the mesoporous silica [22,23] and polyhedral oligomeric silsesquioxane (POSS) [24,25] display outstanding nano-sized structures and are widely applied to decrease the ε and $tan\delta$ values of CE resins. Devaraju [22]

* Corresponding author.,
** Corresponding author.
E-mail addresses: tys@nwpu.edu.cn (Y. Tang), gjw@nwpu.edu.cn, nwpugjw@163.com (J. Gu).
[1] The authors Lin Tang[#] and Junliang Zhang[#] contributed equally to this work and should be considered *co*-first authors.

https://doi.org/10.1016/j.compositesb.2020.107827
Received 6 December 2019; Received in revised form 23 January 2020; Accepted 28 January 2020
Available online 30 January 2020
1359-8368/

et al. reported the addition of 10 wt% functionalized mesoporous silica (GSBA-15) to CE resins could result in a 24% decrease in the ε value (2.53). Jiao [26] et al. synchronously introduced the POSS and mesoporous silica (MPS) into the CE resins to obtain G-POSS-MPS/CE composites. And the ε and *tanδ* values of the G-POSS-MPS/CE composites possessing 4 wt% G-POSS-MPS decreased to 2.78 and 0.008, respectively, comparing with those of pure CE resins (3.27 and 0.012). Although the above methods can effectively reduce the ε and *tanδ* values, the mechanical properties, humidity, as well as heat resistance for the modified CE resins are inevitably decreased. In addition, the design and construction of porous nanostructures are also relatively complicated [27].

C–Si and C–F present low polarizability, small dipoles, and large free volume [28–31], which can be performed to reduce ε and *tanδ* values of CE resins. Zhang [32] et al. adopted hyperbranched siloxane to modify dicyclopentadiene bisphenol cyanate (DCPDCE). The introduction of C–Si could significantly reduce the ε and *tanδ* values. Zhou [33] et al. used 2,2-bis(4-hydroxy-phenyl)-1,1,1,3,3,3-hexafluoropropane and cyanuric chloride to synthesize novel fluorine-containing triazine-based polymers with low ε (2.64) and *tanδ* (0.0025). In our previous work [34], fluorinated compound (TFMPMO) was introduced into the curing networks of bisphenol A cyanate ester (BADCy) resins through copolymerization. Modified BADCy resins possessing 20 wt% of TFMPMO demonstrated low ε and *tanδ* (2.75 and 0.0067), both lower than ε (3.0) and *tanδ* (0.008) of pure BADCy. However, it may cause the severe destruction of the triazine network by introducing a large amount of low-polarity groups (*e.g.* C–Si and C–F) into CE resins, thereby reducing the final mechanical and thermal properties.

Cage-type adamantanes possess excellent hydrophobicity, heat resistance, chemical stability, and good lipid solubility [35–37]. Furthermore, the hydrogen on bridgehead carbons of adamantane presents high activity and can form hydrogen bonds with high electronegative atoms (N and O) [38]. Domagała [39] et al. reported that there were two kinds of hydrogen bonding (C–H···N and C–H···S) in the compound containing adamantane and thiazolidine. In addition, the adamantane exhibits low ε and *tanδ* due to highly symmetric three-membered aliphatic hydrocarbons [40,41]. And it possesses lower cost and easier preparation process [42] compared with that of POSS. Lv [43] et al. reported that a class of super low dielectric porous polyimide (PI) films possessing adamantane groups were obtained through the thermolysis of polyethylene glycol (PEG) oligomers. The porous PI films with ultralow ε value of 1.85 at 1 MHz were obtained. Kong [41] et al. prepared difunctional and trifunctional adamantane benzocyclobutenes (Ada-DVS-BCB and Ada-TVS-BCB), exhibiting low ε (2.5) and *tanδ* (<0.001) over a wide range of frequency.

In this context, designing novel compounds with both cage-type adamantanes and fluorine-containing structures, which are then introduced into the curing networks of BADCy resins *via* copolymerization, is expected to obtain the modified BADCy resins with lower ε and *tanδ* values. Herein, we adopted bisphenol AF, 1-adamantyl chloride, and epichlorohydrin (ECH) as raw materials to obtain the 4-(1,1,1,3,3,3-hexafluoro-2-(4-(epoxy-2-ylmethoxy) phenyl) propan-2-yl) phenyl (*3r*, *5r*, *7r*)-adamantane-1-carboxylate (AEAF) through successive esterification and O-alkylation reaction. AEAF was analyzed and characterized using ^{1}H nuclear magnetic resonance (^{1}H NMR) and Fourier transform infrared (FTIR) spectroscopy. Then, AEAF was copolymerized with BADCy to prepare the modified BADCy (AEAF-*co*-BADCy) resins. AEAF contents influencing on complex permittivity & *tanδ*, wave transmission efficiency, water absorption, heat resistance, mechanical properties, and interfacial compatibility with poly(*p*-phenylene-2,6-benzobisoxazole) (PBO) fibers [44] of the AEAF-*co*-BADCy resins and their PBO fibers/AEAF-*co*-BADCy micor-composites were investigated. And the wave transmission mechanism of the AEAF-*co*-BADCy resins was also simply analyzed.

2. Experimental part

2.1. Synthesis of AEAF

Bisphenol AF (6.72 g, 20 mmol), triethylamine (0.45 g, 4.5 mmol), and dichloromethane (30 mL) were introduced to a flask, and the mixture was stirred for 30 min in an ice bath under nitrogen protection. Then 1-adamantanecarbonyl chloride (0.79 g, 4 mmol) was further added into the above reaction mixture and kept stirring for 12 h. The solvent was then evaporated. The obtained solid was purified using chromatography to yield the ADAF as white powder.

ADAF (1.50 g, 3 mmol), dried potassium carbonate (0.55 g, 4 mmol), ECH (1.38 g, 12 mmol), and acetone (20 mL) were introduced to a flask packed with a condenser. The mixture was stirred at 120 °C for 5 h. Then the reaction mixture was filtered. And the solvent was removed by rotary evaporation to obtain the crude product, followed by purification using chromatography to obtain the AEAF as white powder. The schematic diagram for synthesis route of AEAF is shown in Scheme 1.

2.2. Fabrication of AEAF-co-BADCy resins

A certain amount of AEAF was dissolved into acetone and treated by ultrasonic. Meanwhile, BADCy resins were heated to 150 °C.Then the prepared AEAF solution was mixed with BADCy resins and stirred for 40 min at 150 °C. The AEAF/BADCy mixtures were degassed, which was then poured into a preheated mold at 150 °C. Consequently, the AEAF/BADCy mixtures were cured according to the procedure of 180 °C/2 h +200 °C/5 h, followed by further cured for 2 h at 220 °C. The schematic diagram for preparation of AEAF-*co*-BADCy resins is illustrated in Fig. 1.

The information of the "Main materials" and "Characterizations" details are presented in the "Supporting Information".

3. Results and discussion

3.1. Structural analyses of ADAF and AEAF

Fig. 2 displays the ^{1}H NMR (**a-c**) and FTIR (**d**) spectra of the bisphenol AF, ADAF, and AEAF. In Fig. 2a, three characteristic resonances at 9.04, 7.28, and 6.85 ppm are assigned to the protons for Ar-OH and benzene ring, corresponding to peaks a, b, and c, respectively. ADAF (shown in Fig. 2b) mainly shows proton signals of the adamantane at 1.27–2.07 ppm and the benzene at 6.82–7.43 ppm. Moreover, the benzene rings of ADAF present four protons with different chemical environments at 6.82, 7.11, 7.25, and 7.43 ppm, ascribed to the change in the symmetry of the ADAF structure with introduction of adamantane. After the alkylation reaction between ECH and ADAF, the peak at 9.04 ppm corresponding to phenolic hydroxyl (shown in Fig. 1a–b) disappears in Fig. 1c. The chemical shift at 2.41–4.25 ppm is observed, ascribed to the protons of epoxy groups. According to Fig. 2d, the band around 3300–3400 cm^{-1} and 1350-1120 cm^{-1} for the bisphenol AF can be assigned to the phenolic hydroxyl and –CF_3, respectively. Besides, the vibration peak of benzene ring presents at 1450-1600 cm^{-1}. After introducing adamantane, new characteristic absorption peaks around 2930/2850 cm^{-1} (–CH_2–) and 1760 cm^{-1} (–COO–) both appear, mainly attributed to the introduction of adamantane and the formation of ester bonds. For AEAF, the characteristic absorption peak of epoxy groups (940 cm^{-1}) is also observed. ^{1}H NMR and FTIR analyses indicate that AEAF has been prepared.

3.2. Dielectric properties of AEAF-co-BADCy resins

ε'_r (**a**) and ε''_r (**b**) of the complex permittivity and *tanδ* (**c**, $\varepsilon''_r/\varepsilon'_r$) values of the AEAF-*co*-BADCy resins are displayed in Fig. 3. From Fig. 3a–c, the values of ε'_r, ε''_r, and *tanδ* for AEAF-*co*-BADCy resins are frequency dependent. ε'_r values for AEAF-*co*-BADCy resins are lower and decrease by increasing the frequency, compared to pure BADCy.

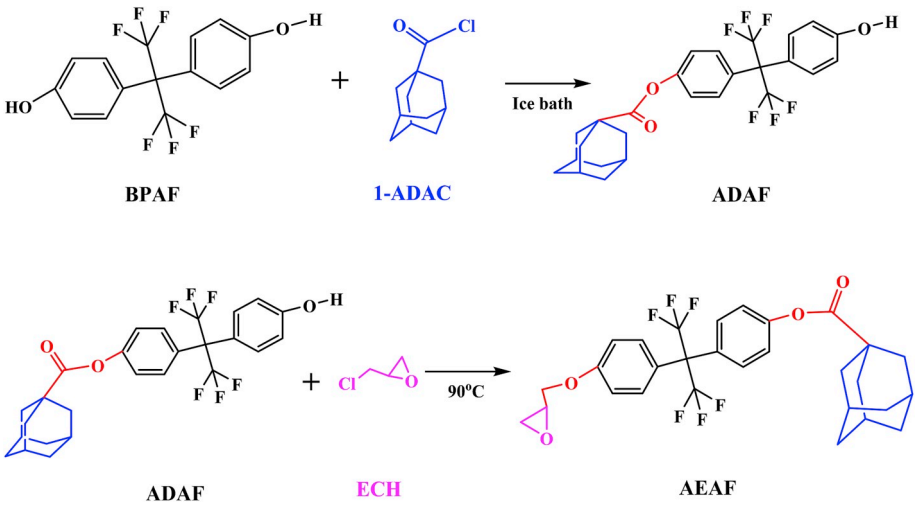

Scheme 1. Schematic diagram for synthesis route of AEAF.

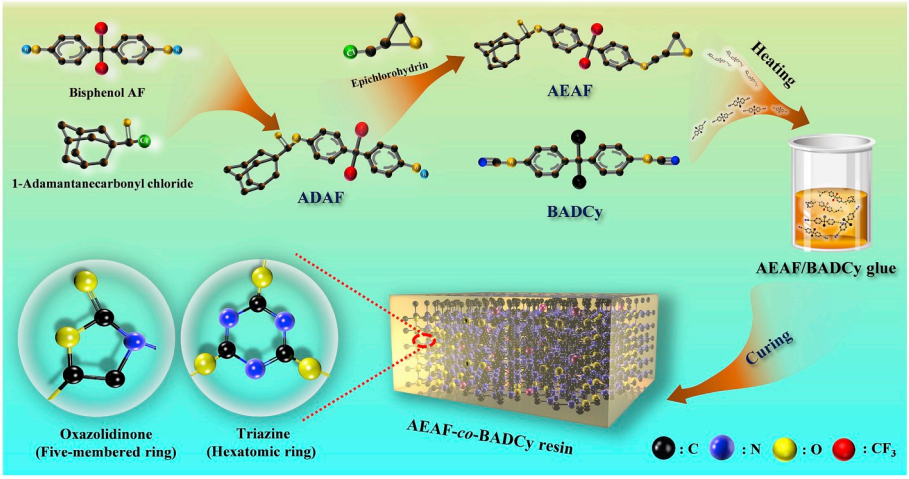

Fig. 1. Schematic diagram of preparation for AEAF-*co*-BADCy resins.

Conversely, the ε''_r and *tanδ* values steadily increase while increase the frequency. The reason is that all the polarization (electronic, atomic, and orientation polarization) of the AEAF-*co*-BADCy resins can keep up with the changing electromagnetic field and the polarization loss is less. However, as the frequency of the electromagnetic waves increases, the orientation polarization can no longer catch up with the electric field change and then disappears. Thus, the ε'_r of AEAF-*co*-BADCy resins reduces. When the frequency of the electromagnetic waves is close to the natural vibration frequency of the atomic polarization and electron polarization, the AEAF-*co*-BADCy resins can absorb more electric field energy, thereby increasing the ε''_r and *tanδ*.

In addition, ε'_r, ε''_r and *tanδ* values for AEAF-*co*-BADCy resins all decrease first and then increase as the content of AEAF increases. When the mass fraction of AEAF was 6 wt%, the ε'_r, ε''_r, and *tanδ* values for AEAF-*co*-BADCy resins all display the minimum values, which are 2.49, 0.012, and 0.0048, respectively (10 GHz), and much higher than pure BADCy (ε'_r of 2.93, ε''_r of 0.019 and *tanδ* of 0.0065, 10 GHz). According to the Debye theory [34], the ε'_r is essentially related to the amount of polarization occurring inner polymer matrix and the ε''_r intrinsically reflects the capacity of dielectric loss. On one hand, the CF_3 groups present lower polarizability and larger free volume. On the other hand, the adamantyl groups exhibit nanometer sized holes, which both can effectively reduce the polarizability and dipole density, resulting further decrease of ε'_r, ε''_r, and *tanδ* based on Clausius-Mosotti equation [34] ((Equation (1), the ε decreases with decreasing polarizability and dipole density).

$$\varepsilon = 1+3N\alpha/(3\varepsilon_0 - N\alpha) \quad (1)$$

Where, N and α represent the number of molecules per unit dielectric volume and polarizability, respectively. However, excessive epoxy groups in AEAF (8 wt%) can react with –OCN groups to destroy regular structures of triazine-ring and form a large number of polar oxazolidinyl structures (shown in Scheme S1). Therefore, the corresponding values of ε'_r, ε''_r, and *tanδ* for AEAF-*co*-BADCy resins are increased.

What's more, when the electromagnetic waves are incident on the AEAF-*co*-BADCy resins, the relationship of reflection coefficient (***Γ***), energy loss (***A***), and wave transmission coefficient (***T***) is shown in Equation (2):

$$\Gamma + A + T = 1 \quad (2)$$

Γ and T are obtained from the network analyzer in form of scattering parameter "S_{mn}", which measures the energy scattering from a material or device. Γ and T coefficients can be calculated using the Equations (3) and (4) [45].

$$\Gamma = |S_{11}|^2 = |S_{22}|^2 \quad (3)$$

$$T = |S_{12}|^2 = |S_{21}|^2 \quad (4)$$

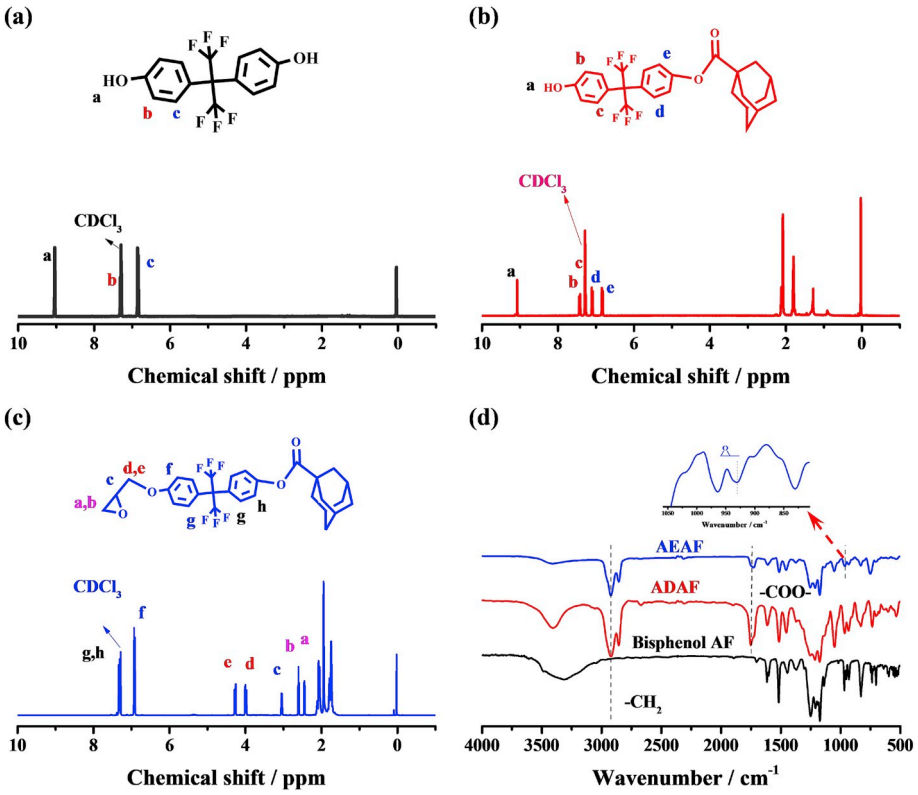

Fig. 2. ^{1}H NMR (a–c) and FTIR (d) spectra of bisphenol AF, ADAF and AEAF.

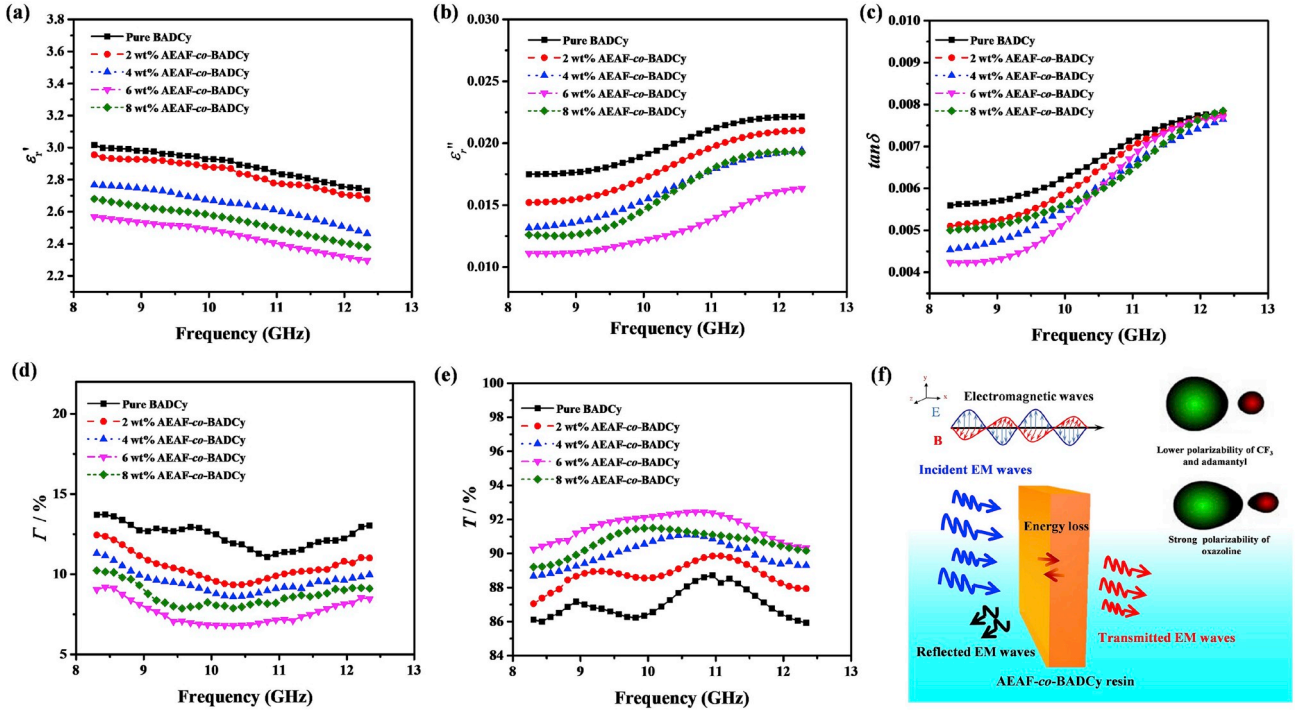

Fig. 3. AEAF contents affecting on the ε'_r (a), ε''_r (b) and *tanδ* (c) values of AEAF-*co*-BADCy resins; Reflection coefficient (d); Wave transmission efficiency (e); Schematic diagram of electromagnetic waves transmission (f).

Γ and *T* of the AEAF-*co*-BADCy resins are illustrated in Fig. 3d–e. *Γ* of the AEAF-*co*-BADCy resins decrease first and then increase as the content of AEAF increases, but the change of *T* is opposite to that of *Γ*. AEAF-*co*-BADCy resins possessing 6 wt% AEAF present the maximum *T* value of 92.3% (10 GHz), higher than that of pure BADCy (86.6%). Respective *Γ* decreases from 12.8% (pure BADCy) to 6.8% and the corresponding A is less than 1%. The reason is that AEAF-*co*-BADCy resins are the insulator (no electrical loss and magnetic loss) and the transmission loss of

electromagnetic waves is mainly dielectric loss (transmission diagram shown in Fig. 3f). In addition, based on the impedance matching theory [46], the lower ε'_r values of the AEAF-*co*-BADCy resins, the smaller the difference of impedance between the load phase (AEAF-*co*-BADCy resins) and transport phase (air), which results in weaker interface reflection, and further increases the *T* values.

3.3. Density and hydrophobicity of AEAF-co-BADCy resins

Fig. 4 demonstrates the influence of AEAF contents on the density (**a**), water absorption rate (**b**), and contact angles (**c**) of the AEAF-*co*-BADCy resins. The density of AEAF-*co*-BADCy resins is gradually decreased with the increasing addition of AEAF. And the density of AEAF-*co*-BADCy resins possessing 6 wt% AEAF is 1.15 g/cm^3, which is lower in comparison with pure BADCy (1.18 g/cm^3). The main reason is that the adamantane possesses lower density (1.07 g/cm^3), thereby effectively reducing the final density of AEAF-*co*-BADCy resins. In addition, excessive AEAF can destroy regular triazine-ring structures and reduce packing density of the curing networks, beneficial to reducing the density. From Fig. 4b, the water absorption contents of the pure BADCy and AEAF-*co*-BADCy resins improve by prolonging the immersion time and become stable after 36 h. This is mainly due to the water diffusion from the surface of AEAF-*co*-BADCy resins into the interior, resulting in increased water absorption. When the system reaches the saturation state, the water absorption tends to be stable. Moreover, at the same dipping time, the water absorption of AEAF-*co*-BADCy resins decreases and the contact angle gradually increases (shown in Fig. 4c) with the increase of AEAF amount. Contact angle of 5 μL water droplets on the AEAF-*co*-BADCy resins possessing 6 wt% AEAF increases to 111.5°, which is higher compared with pure BADCy (95.2°). This can be attributed that CF_3 presents low surface tension and high hydrophobicity [47] and fully aliphatic adamantane-enriched –CH– also possesses good hydrophobicity. Thus, AEAF is beneficial to reducing surface energy of AEAF-*co*-BADCy resins (shown in Fig. 4d), resulting in higher contact angles and lower water absorption.

3.4. Thermal properties of AEAF-co-BADCy resins

Fig. 5 presents the TGA (**a**) and DMA (**b** and **b'**) curves for pure BADCy and AEAF-*co*-BADCy resins. And the corresponding thermal information are summarized in Table 1. T_g values for AEAF-*co*-BADCy resins are determined by peak temperature of *tanδ* (shown in Fig. 5b'). From Table 1, AEAF-*co*-BADCy resins present higher calculated heat resistance index (T_{HRI}) compared to pure BADCy. T_{HRI} values for AEAF-*co*-BADCy resins increase initially, followed by decreasing as the content of AEAF increases. AEAF-*co*-BADCy resins possessing 6 wt% AEAF present the maximum T_{HRI} value of 217.9 °C, 5.1% higher compared to pure BADCy (207.3 °C). The storage modulus (shown in Fig. 5b) and T_g (shown in Table 1) values also increase firstly, but then decrease with the increasing addition of AEAF. AEAF-*co*-BADCy resins with 6 wt% AEAF possess the maximum T_g value of 276.3 °C, 8.7% higher than that of pure BADCy (254.1 °C). The reason is that rigid adamantane and CF_3 present excellent thermal stabilities, beneficial to enhancing the storage modulus and heat resistance. Furthermore, the large volume of rigid AEAF is embedded into BADCy cross-linking networks *via* copolymerization, so as to restrict the rotation and movement of the molecular chains, resulted in the increased T_g values. However, the excessive oxazolinone fragments from polycyanurate networks will reduce T_{HRI}, storage modulus, and T_g values for AEAF-*co*-BADCy resins.

To further elucidate the effects of excessive AEAF contents on reducing the T_g of AEAF-*co*-BADCy resins, Equation (5) for rubbery plateau storage modulus at T_g + 40 °C is used to calculate the cross-linking density [48,49], and the calculation results are shown in Fig. 5c.

$$d_{cross\text{-}link} = E'/2(1+\gamma)RT \quad (5)$$

Where, E′ is storage modulus of AEAF-*co*-BADCy resins at temperature *T* (T_g+40 °C), R represents gas constant, and γ represents Poisson's ratio, which is assumed to be 0.5 for incompressible networks.

From Fig. 5c, the crosslinking density of AEAF-*co*-BADCy resins reduces as the AEAF content increases. On one hand, the decreased crosslinking density of AEAF-*co*-BADCy resins will reduce T_g values. On the other hand, a large volume of rigid adamantane restricts the rotation and movement of the molecular chains, resulted in increased T_g values.

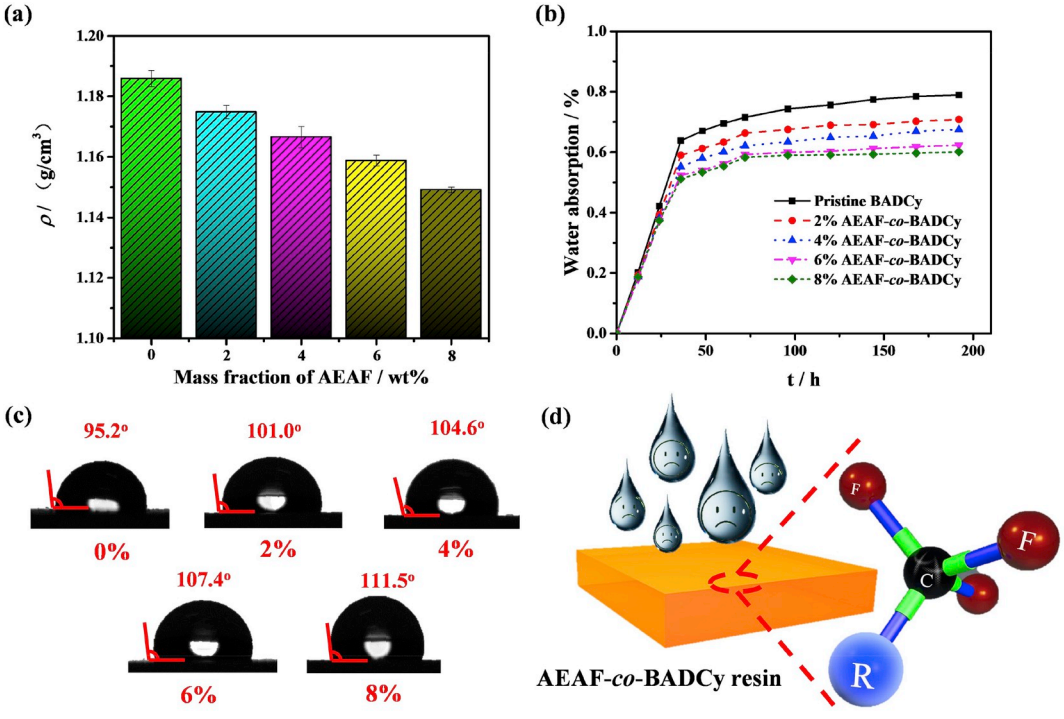

Fig. 4. Density (a), water absorption (b) and contact angles (c) of pure BADCy and AEAF-*co*-BADCy resins.

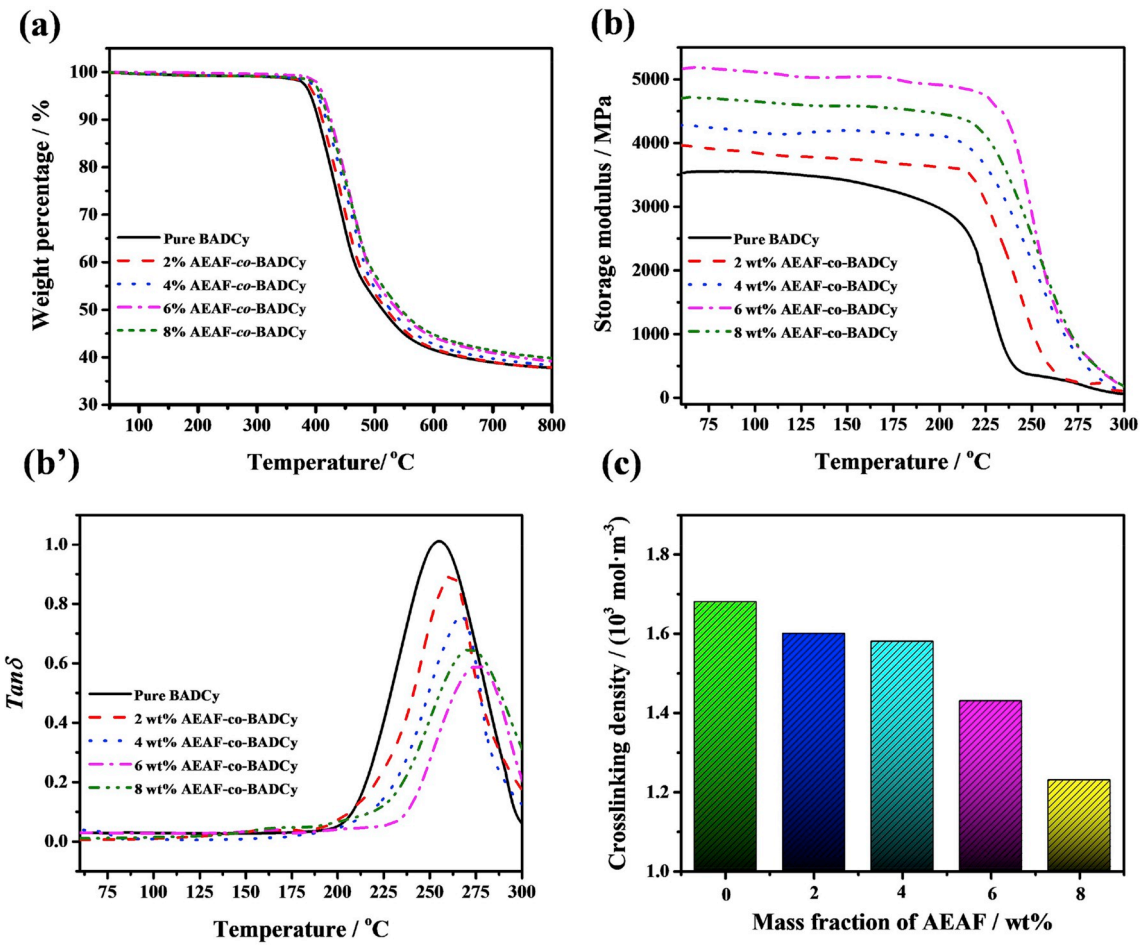

Fig. 5. TGA (a), DMA (b, b'), and crosslinking density (c) of pure BADCy and AEAF-*co*-BADCy resins.

Table 1
Thermal data of pure BADCy and AEAF-*co*-BADCy resins.

Samples	Weight loss Temperature/ oC		THeat-resistance index*/ oC	Tg/oC
	5%	30%		
Pure BADCy	391.3	444.3	207.3	254.1
2 wt% AEAF-*co*-BADCy	398.5	449.0	210.1	261.4
4 wt% AEAF-*co*-BADCy	404.6	459.3	214.3	266.9
6 wt% AEAF-*co*-BADCy	413.6	465.7	217.9	276.3
8 wt% AEAF-*co*-BADCy	407.5	462.7	215.9	270.6

$T_{Heat\text{-}resistance\ index} = 0.49 \times [T_5 + 0.6 \times (T_{30} - T_5)]$ (Equation (6)) [50].
T_5 and T_{30} are the corresponding decomposition temperature of 5% and 30% weight loss, respectively.

When the amount of AEAF exceeds 6 wt%, the former presents a greater effect on the T_g values. Thus, the corresponding T_g values increase firstly, but then decrease with the increasing addition of AEAF.

3.5. Mechanical properties of the AEAF-co-BADCy resins and their interfacial compatibilities with PBO fibers

Fig. 6a shows the amount of AEAF affecting on the mechanical properties for AEAF-*co*-BADCy resins. Flexural strength and impact strength of AEAF-*co*-BADCy resins are steadily increased as the AEAF amount increases. In comparison with pure BADCy (108.5 MPa for flexural strength and 10.3 kJ m^{-2} for impact strength), and AEAF-*co*-BADCy resins possessing 6 wt% AEAF are increased to 126.5 MPa for flexural strength and 15.2 kJ m^{-2} for impact strength, improved by 16.6% and 47.6%, respectively. The reason is that the introduction of adamantane with rigidity and low ring strain increases the overall rigidity of the AEAF-*co*-BADCy resins, resulted in the enhanced flexural strength. Moreover, due to monofunctional epoxy group of AEAF, the crosslinking network chain ends at AEAF. Therefore, the large volume of AEAF compounds can be regarded as a node inner crosslinking networks to effectively transfer stress and prevent crack propagation (shown in Fig. 6d–h, the degree of stress whitening and roughness of impact fractures), thus increasing the impact strength for AEAF-*co*-BADCy resins.

Fig. 6b shows the amount of AEAF affecting on the interfacial compatibility of PBO fibers/AEAF-*co*-BADCy micro-composites. Single fiber pull-out strength of the micro-composites rises as the AEAF content increases. Single fiber pull-out strength of the PBO fibers/AEAF-*co*-BADCy micro-composites with 6 wt% AEAF is increased to 3.4 MPa, increased by 9.6%, compared with that of the PBO fibers/BADCy micro-composites (3.1 MPa). This is mainly attributed to poor interfacial compatibility between BADCy resins and PBO fibers [51,52]. Consequently, PBO fibers/BADCy micro-composites present lower single fiber pull-out strength (shown in Fig. 6d', the surface of PBO fibers is very smooth and no residual BADCy resins attached). Also, adamantyl group has better affinity with benzene ring of PBO fibers. In addition, the highly active hydrogen on the bridgehead carbon of the adamantane may be combined with N and O of the oxazole ring of the PBO fibers as hydrogen bonds (shown in Fig. 6c), which further improves the

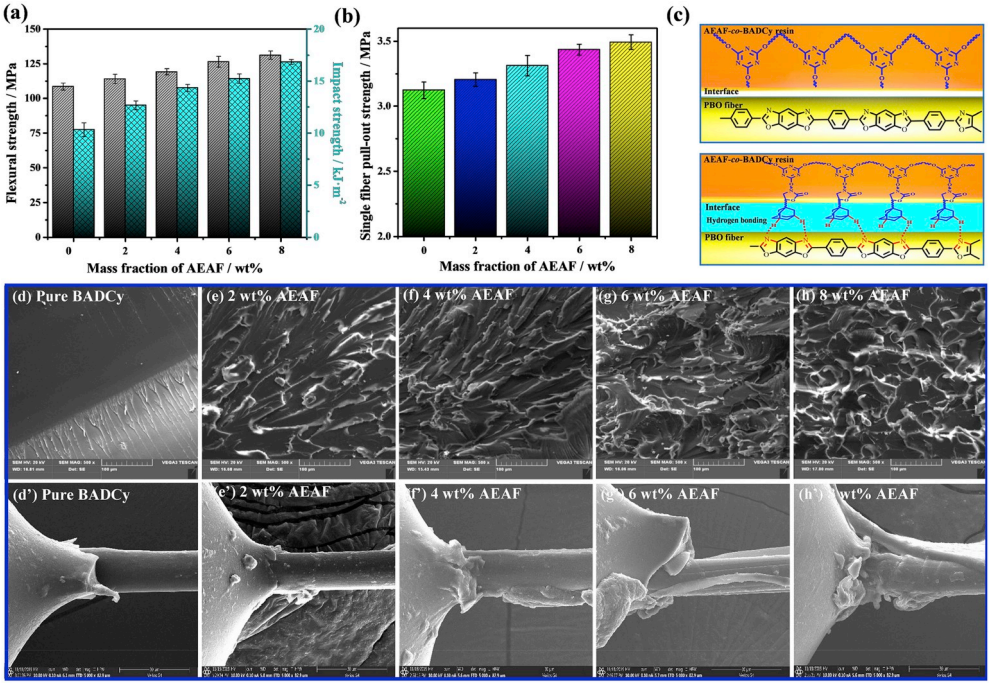

Fig. 6. Mechanical properties of pure BADCy and AEAF-*co*-BADCy resins (a); Single fiber pull-out strength of the PBO fibers/BADCy and PBO fibers/AEAF-*co*-BADCy micro-composites (b); Schematic diagram of the interfaces for PBO fibers/BADCy and PBO fibers/AEAF-*co*-BADCy micro-composites (c); SEM morphologies of impact fractures for BADCy and AEAF-*co*-BADCy resins (d–h); SEM images of the PBO fibers surfaces after single fiber pull-out test (d'-h').

interfacial compatibility between the AEAF-*co*-BADCy resins and PBO fibers (shown in Fig. 6e'-h', the residual AEAF-*co*-BADCy resins attached on the surface of the PBO fibers increase as the amount of AEAF increases).

4. Conclusions

^{1}H NMR and FTIR analyses indicated that AEAF was successfully synthesized and the five-member ring oxazolinoline was formed inner crosslinking networks of the AEAF-*co*-BADCy resins. AEAF with low polarizability, dipole density, rigid cage adamantane, and stable CF_3 endued the AEAF-*co*-BADCy resins excellent comprehensive properties. AEAF-*co*-BADCy resins with 6 wt% AEAF possessed the minimum ε'_r, ε''_r, and *tanδ* values, which were 2.49, 0.012, and 0.0048, respectively (10 GHz). The wave transmission efficiency (*T*) was 92.3%, significantly higher in comparison with pure BADCy (86.6%). Moreover, it presented the optimal thermal stability (T_{HRI} of 217.9 °C) and the highest T_g value (276.3 °C), increased by 5.1% and 8.7%, respectively, in comparison with pure BADCy (T_{HRI} of 207.3 °C and T_g of 254.1 °C). AEAF-*co*-BADCy resins also displayed excellent mechanical properties and better interfacial compatibilities with PBO fibers. Flexural strength (126.5 MPa) and impact strength (15.2 kJ m^{-2}) for AEAF-*co*-BADCy resins possessing 6 wt% AEAF increased by 16.6% and 47.6%, respectively, in comparison with pure BADCy (108.5 MPa for flexural strength and 10.3 kJ m^{-2} for impact strength). Single fiber pull-out strength of PBO fibers/AEAF-*co*-BADCy micro-composites with 6 wt% AEAF improved to 3.4 MP from 3.1 MPa for PBO fibers/BADCy micro-composites.

Declaration of competing interest

The authors declare that they have no known competing financial interests or personal relationships that could have appeared to influence the work reported in this paper.

CRediT authorship contribution statement

Lin Tang: Conceptualization, Writing - original draft. **Junliang Zhang:** Methodology, Formal analysis. **Yusheng Tang:** Supervision. **Yuxiao Zhou:** Data curation. **Yuhan Lin:** Project administration. **Zheng Liu:** Investigation, Funding acquisition. **Jie Kong:** Writing - review & editing. **Tianxi Liu:** Validation. **Junwei Gu:** Supervision.

Acknowledgements

This work is supported by Space Supporting Fund from China Aerospace Science and Industry Corporation (2019-HT-XG); China Postdoctoral Science Foundation (2019M653735); Fundamental Research Funds for the Central Universities (310201911py010 and 310201911qd003); Open Fund from Henan University of Science and Technology; State Key Laboratory for Modification of Chemical Fibers and Polymer Materials from Donghua University (KF2001); Y.H. Lin thanks for the Undergraduate Innovation & Business Program in Northwestern Polytechnical University (S201910699186). We would like to thank the Analytical & Testing Center of Northwestern Polytechnical University for SEM tests.

Appendix A. Supplementary data

Supplementary data to this article can be found online at https://doi.org/10.1016/j.compositesb.2020.107827.

References

[1] Zhang Z, Yuan L, Liang G, Gu A, Qiang Z, Yang C, Chen X. Unique hybridized carbon nanotubes and their high performance flame retarding composites with high smoke suppression, good toughness and low curing temperature. J Mater Chem 2014;2(14):4975–88.
[2] Tang L, Dang J, He M, Li J, Kong J, Tang Y, Gu J. Preparation and properties of cyanate-based wave-transparent laminated composites reinforced by dopamine/POSS functionalized Kevlar cloth. Compos Sci Technol 2019;169:120–6.
[3] Zhang S, Yan Y, Li X, Fan H, Ran Q, Fu Q, Gu Y. A novel ultra low-k nanocomposites of benzoxazinyl modified polyhedral oligomeric silsesquioxane and cyanate ester. Eur Polym J 2018;103:124–32.

[4] Yuan L, Huang S, Gu A, Liang G, Chen F, Hu Y, Nutt S. A cyanate ester/microcapsule system with low cure temperature and self-healing capacity. Compos Sci Technol 2013;87:111–7.
[5] Triki A, Guicha M, Ben Hassen M, Arous M, Fakhfakh Z. Studies of dielectric relaxation in natural fibres reinforced unsaturated polyester. J Mater Sci 2011;46(11):3698–707.
[6] Zhang Q, Guan Q, Yuan L, Gu A, Liang G. A very low concentration of polybenzimidazole film interleaved bismaleimide/diallyl bisphenol a system with outstanding improvement in impact strength and excellent allround properties. Polym Compos 2018;39(12):4569–80.
[7] Song N, Yao H, Ma T, Wang T, Shi K, Tian Y, Zhang B, Zhu S, Zhang Y, Guan S. Decreasing the dielectric constant and water uptake by introducing hydrophobic cross-linked networks into co-polyimide films. Appl Surf Sci 2019;480:990–7.
[8] Li Y, Wang Z, Zhan Y, Wang S, Tao X, Liao C, Lu Z. Improved mechanical and dielectric performances of epoxy nanocomposites filled with aminated polyethylene glycol grafted graphene. Mater Lett 2019;246:149–52.
[9] Bershtein V, Fainleib A, Gusakova K, Kirilenko D, Yakushev P, Egorova L, Lavrenyuk N, Ryzhov V. Silica subnanometer-sized nodes, nanoclusters and aggregates in Cyanate Ester Resin-based networks: structure and properties of hybrid subnano- and nanocomposites. Eur Polym J 2016;85:375–89.
[10] Ohashi S, Pandey V, Arza CR, Froimowicz P, Ishida H. Simple and low energy consuming synthesis of cyanate ester functional naphthoxazines and their properties. Polym Chem 2016;7(12):2245–52.
[11] Gu J, Li Y, Liang C, Tang Y, Tang L, Zhang Y, Kong J, Liu H, Guo Z. Synchronously improved dielectric and mechanical properties of wave-transparent laminated composites combined with outstanding thermal stability by incorporating iysozyme/POSS functionalized PBO fibers. J Mater Chem C 2018;6(28):7652–60.
[12] Han J, Liang G, Gu A, Ye J, Zhang Z, Yuan L. A novel inorganic–organic hybridized intumescent flame retardant and its super flame retarding cyanate ester resins. J Mater Chem 2013;1(6):2169–82.
[13] Li Y, Xu G, Guo Y, Ma T, Zhong X, Zhang Q, Gu J. Fabrication, proposed model and simulation predictions on thermally conductive hybrid cyanate ester composites with boron nitride fillers. Composites Part A 2018;107:570–8.
[14] Wu H, Rogalski M, Kessler MR. Zirconium tungstate/epoxy nanocomposites: effect of nanoparticle morphology and negative thermal expansivity. ACS Appl Mater Interfaces 2013;5(19):9478–87.
[15] Chen S, Yuan L, Wang Z, Gu A, Liang G. Self-constructed nanodomain structure in thermosetting blend based on the dynamic reactions of cyanate ester and epoxy resins and its related property. Compos B Eng 2019;177:107438.
[16] Guan Q, Yuan L, Zhang Y, Gu A, Liang G. Improving the mechanical, thermal, dielectric and flame retardancy properties of cyanate ester with the encapsulated epoxy resin-penetrated aligned carbon nanotube bundle. Compos B Eng 2017;123:81–91.
[17] Tang Y, Dong W, Tang L, Zhang Y, Kong J, Gu J. Fabrication and investigations on the polydopamine/KH-560 functionalized PBO fibers/cyanate ester wave-transparent composites. Compos Commun 2018;8:36–41.
[18] Liu Z, Zhang J, Tang L, Zhou Y, Lin Y, Wang R, Kong J, Tang Y, Gu J. Improved wave-transparent performances and enhanced mechanical properties for fluoride-containing PBO precursor modified cyanate ester resins and their PBO fibers/cyanate ester composites. Compos B Eng 2019;178:107466.
[19] Li X, Zhang P, Dong J, Gan F, Zhao X, Zhang Q. Preparation of low-κ polyimide resin with outstanding stability of dielectric properties versus temperature by adding a reactive Cardo-containing diluent. Compos B Eng 2019;177:107401.
[20] Zhang K, Yu X, Kuo S. Outstanding dielectric and thermal properties of main chain-type poly(benzoxazine-co-imide-co-siloxane)-based cross-linked networks. Polym Chem 2019;10(19):2387–96.
[21] Fang L, Zhou J, Tao Y, Wang Y, Chen X, Chen X, Hou J, Sun J, Fang Q. Low dielectric fluorinated polynorbornene with good thermostability and transparency derived from a biobased allylphenol (eugenol). ACS Sustainable Chem Eng 2019;7(4):4078–86.
[22] Devaraju S, Vengatesan MR, Selvi M, Song JK, Alagar M. Mesoporous silica reinforced cyanate ester nanocomposites for low k dielectric applications. Microporous Mesoporous Mater 2013;179:157–64.
[23] Gürgen S. Wear performance of UHMWPE based composites including nano-sized fumed silica. Compos B Eng 2019;173:106967.
[24] Wang J, Wei Y, Li X, Mu J. Ultra-low dielectric constant materials with hydrophobic property: synthesis of poly(aryl ether sulfone) with POSS and biphenyl group in the main chain. High Perform Polym 2019;31(5):503–12.
[25] Li W, Huang W, Kang Y, Gong Y, Ying Y, Yu J, Zheng J, Qiao L, Che S. Fabrication and investigations of G-POSS/cyanate ester resin composites reinforced by silane-treated silica fibers. Compos Sci Technol 2019;173:7–14.
[26] Jiao J, Zhao L, Wang L, Lv P, Cui Y, Wu G. A novel hybrid functional nanoparticle and its effects on the dielectric, mechanical, and thermal properties of cyanate ester. Polym Compos 2016;37(7):2142–51.
[27] Deng G, Wang Z. Triptycene-based microporous cyanate resins for adsorption/separations of benzene/cyclohexane and carbon dioxide gas. ACS Appl Mater Interfaces 2017;9(47):41618–27.
[28] Wang Y, Wang J, Jin K, Sun J, Fang Q. A new glass-forming molecule having a fluorene skeleton: synthesis and conversion to the polymer with a low dielectric constant, high hydrophobicity and thermostability. Polym Chem 2016;7(38):5925–9.
[29] Wang K, Hu N, Xu G, Qi Y. Stable superhydrophobic composite coatings made from an aqueous dispersion of carbon nanotubes and a fluoropolymer. Carbon 2011;49(5):1769–74.
[30] Galli S, Cimino A, Ivy JF, Giacobbe C, Arvapally RK, Vismara R, Checchia S, Rawshdeh MA, Cardenas CT, Yaseen WK, Maspero A, Omary MA. Fluorous metal–organic frameworks and nonporous coordination polymers as low-κ dielectrics. Adv Funct Mater 2019;29(40):1904707.
[31] Dong Z, Ni Y, Yang X, Hu C, Sun J, Li L, Zhou C, Fan H. Characterization and analysis of fluoride calcium silicate composite interface in remineralization of dental enamel. Compos B Eng 2018;153:393–7.
[32] Zhang MM, Yan HX, Gong C, Li TT. Hyperbranched polysiloxane functionalized graphene oxide for dicyclopentadiene bisphenol dicyanate ester nanocomposites with high performance. Express Polym Lett 2014;8(6):413–24.
[33] Zhou J, Wang J, Tao Y, Fang L, Sun J, Fang Q. New triazine-based polymers with low dielectric constants and high thermostability derived from biorenewable anethole and thermocrosslinkable benzocyclobutene. ACS Sustainable Chem Eng 2018;6(4):5620–6.
[34] Gu J, Dong W, Tang Y, Guo Y, Tang L, Kong J, Tadakamalla S, Wang B, Guo Z. Ultralow dielectric, fluoride-containing cyanate ester resins with improved mechanical properties and high thermal and dimensional stabilities. J Mater Chem C 2017;5(28):6929–36.
[35] Schwertfeger H, Fokin AA, Schreiner PR. Diamonds are a chemist's best friend: diamondoid chemistry beyond adamantane. Angew Chem Int Ed 2008;47(6):1022–36.
[36] Aguilar-Lugo C, Álvarez C, Lee YM, de la Campa JG, Lozano Á E. Thermally rearranged polybenzoxazoles containing bulky adamantyl groups from ortho-substituted precursor copolyimides. Macromolecules 2018;51(5):1605–19.
[37] Ree BJ, Kobayashi S, Heo K, Lee TJ, Satoh T, Ishizone T, Ree M. Nanoscale film morphology and property characteristics of dielectric polymers bearing monomeric and dimeric adamantane units. Polymer 2019;169:225–33.
[38] Kakuta T, Takashima Y, Sano T, Nakamura T, Kobayashi Y, Yamaguchi H, Harada A. Adhesion between semihard polymer materials containing cyclodextrin and adamantane based on host–guest interactions. Macromolecules 2015;48(3):732–8.
[39] Domagała M, Grabowski SJ, Urbaniak K, Mlostoń G. Role of C−H···S and C−H···N hydrogen bonds in organic crystal StructuresThe crystal and molecular structure of 3-Methyl-2,4-diphenyl-(1,3)-thiazolidine-5-spiro-2'-adamantane and 3-Methyl-2,4,5,5-tetraphenyl-(1,3)-thiazolidine. J Phys Chem 2003;107(15):2730–6.
[40] Fu D-W, Zhao M-M, Ge J-Z. Synthesis, structure and dielectric property of two H-bonded supramolecular compounds with 1-aminoadamantane based on 18-crown-6. J Mol Struct 2011;1006(1–3):227–33.
[41] Kong L, Cheng Y, Jin Y, Ren Z, Li Y, Xiao F. Adamantyl-based benzocyclobutene low-k polymers with good physical properties and excellent planarity. J Mater Chem C 2015;3(14):3364–70.
[42] Yang H-B, Feceu A, Martin DBC. Catalyst-controlled C–H functionalization of adamantanes using selective H-atom transfer. ACS Catal 2019;9(6):5708–15.
[43] Lv P, Dong Z, Dai X, Wang H, Qiu X. Synthesis and properties of ultralow dielectric porous polyimide films containing adamantane. Polym Chem 2018;56(5):549–59.
[44] Chen L, Hu Z, Wu Z, Wu G, Ma L, Zhang C, Huang Y. POSS-bound ZnO nanowires as interphase for enhancing interfacial strength and hydrothermal aging resistance of PBO fiber/epoxy resin composites. Composites Part A 2017;96:1–8.
[45] Faisal S, Mohamed A, Christine B, Babak A, Soon M, Chong M, Yury G. Electromagnetic interference shielding with 2D transition metal carbides (MXenes). Science 2016;353(6304):1137–40.
[46] Osipov AV. Minimum reflection properties of planar impedance-matched boundaries. IEEE Trans Antenn Propag 2014;62(11):5666–70.
[47] Jiang D, Guo F, Xu M, Cai J, Cong S, Jia M, Chen G, Song Y. Conformal fluorine coated carbon paper for an energy harvesting water wheel. Nano Energy 2019;58:842–51.
[48] Ohashi S, Kilbane J, Heyl T, Ishida H. Synthesis and characterization of cyanate ester functional benzoxazine and its polymer. Macromolecules 2015;48(23):8412–7.
[49] Wang Y, Kou K, Wu G, Zhuo L, Li J, Zhang Y. The curing reaction of benzoxazine with bismaleimide/cyanate ester resin and the properties of the terpolymer. Polymer 2015;77:354–60.
[50] Yang X, Fan S, Li Y, Guo Y, Li Y, Ruan K, Zhang S, Zhang J, Kong J, Gu J. Synchronously improved electromagnetic interference shielding and thermal conductivity for epoxy nanocomposites by constructing 3D copper nanowires/thermally annealed graphene aerogel framework. Composites Part A 2020;128:105670.
[51] Hu Z, Lu F, Liu Y, Zhao L, Yu L, Xu X, Yuan W, Zhang Q, Huang Y. Construction of anti-ultraviolet "shielding clothes" on poly(p-phenylene benzobisoxazole) fibers: metal organic framework-mediated absorption strategy. ACS Appl Mater Interfaces 2018;10(49):43262–74.
[52] Hu Z, Shao Q, Huang Y, Yu L, Zhang D, Xu X, Lin J, Liu H, Guo Z. Light triggered interfacial damage self-healing of poly(p-phenylene benzobisoxazole) fiber composites. Nanotechnology 2018;29(18):185602.